Journal Of Agricultural And Food Chemistry
September 2021, Volume 69 Issue 37 Pages 10893-10906
https://doi.org/10.1021/acs.jafc.1c03141
https://archimer.ifremer.fr/doc/00727/83935/

Identification of Antagonistic Compounds between the Palm Tree Xylariale Endophytic Fungi and the Phytopathogen *Fusarium oxysporum*

Barthélemy Morgane [1], Elie Nicolas [1], Genta-Jouve Grégory [2], Stien Didier [3], Touboul David [1, *], Eparvier Véronique [1, *]

[1] Univ Paris Saclay, Inst Chim Subst Nat, CNRS, UPR 2301, F-91198 Gif Sur Yvette, France.
[2] Univ Guyane, Lab Ecol Evolut Interact Syst Amazoniens LEEISA, CNRS Guyane, USR 3456, Cayenne 97300, French Guiana.
[3] UPMC Univ Paris 06, Observ Oceanol, Lab Biodiversite & Biotechnol Microbiennes LBBM, Sorbonne Univ,CNRS, F-66650 Banyuls Sur Mer, France.

Corresponding authors : David Touboul, email address : david.touboul@cnrs.fr ; Véronique Eparvier, email address : veronique.eparvier@cnrs.fr

Abstract :

To discover microorganisms that naturally possess chemical weapons against the phytopathogen Fusarium oxysporum, the biological and chemical diversity of plant leaf endophytes was investigated. Endophytes were isolated from the palm tree Astrocaryum sciophyllum collected in pristine forests of French Guiana. Several Xylariaceae inhibited the growth of F. oxysporum and were further explored. Antifungal specialized metabolites were isolated from the Xylariaceae BSNB-0294 strain in confrontation with the phytopathogen and led to the identification of undescribed compounds, i.e., two depsipeptides named xylariaceins, two metabolites containing a 3-imidazolinone moiety, and four new compounds including a nitro-phenylpropanamide and three phenylalanine analogues named xylariains A-D. In parallel, the chemical investigation of the phytopathogen during the coculture led to the identification of an unknown compound, which we named focicin. The production of focicin was exacerbated during the competition. Matrix-assisted laser desorption/ionization coupled to time-of-flight mass spectometry (MALDI-TOF MS) imaging of the competition between BSNB-0294 (endophytic strain) and F. oxysporum f.sp. ciceris (phytopathogen) highlighted time-dependent chemical interactions between the two microorganisms.

Graphical abstract

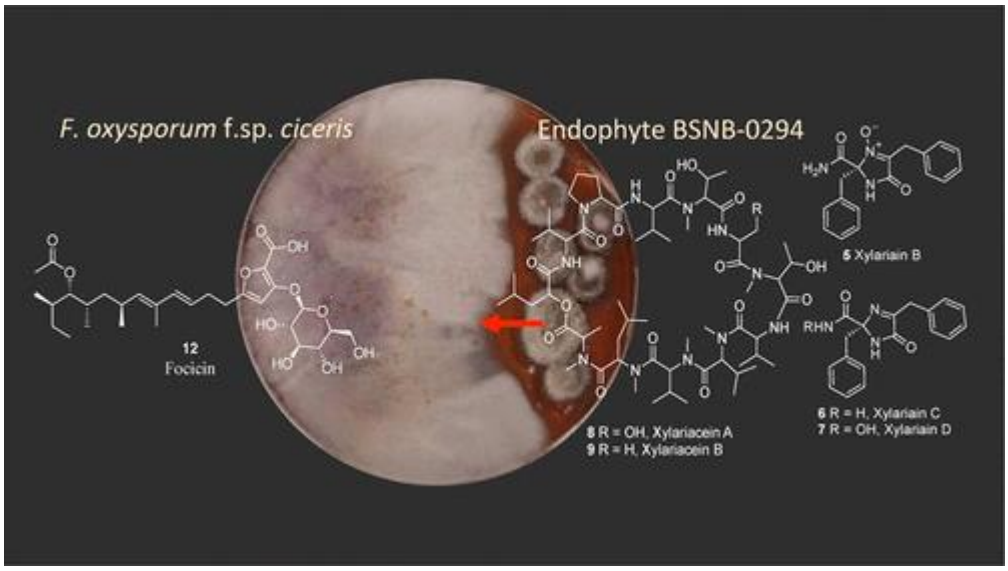

Keywords : endophyte, Xylariale, phytopathogen, Fusarium sp., natural products, molecular network, MALDI-TOF MS imaging

Fusarium oxysporum is a fungus widespread in soils. The species includes both nonpathogenic and economically important plant pathogens. Pathogenic strains of *F. oxysporum* have been intensively studied; the host range of these fungi is broad and includes animals from arthropods to humans, as well as plants.[1-3] Nevertheless, individual isolates usually cause disease only in a narrow range of plant species. This observation has led to the idea of a "special form" or *formae specialis* in *F. oxysporum*. These special forms indicate the specialization of the fungus towards the infected species or even plant cultivar. Exhaustive host range studies have been conducted for relatively few *formae speciales* of *F. oxysporum.*[4] The best-known and most feared form in agronomy is *F. oxysporum* f. sp. *cubense* causing fusarium wilt.[5] To date, 106 other fungal special forms have been characterized, and many are attacking crops such as cotton (f.sp. *vasinfectum*), soybeans (f.sp. *wisteria*), tomatoes (f.sp. *lycopersici*), melon (f.sp. *niveum*), spinach (f.sp. *betae*) or chickpea (f sp. *ciceris*). In addition to banana (f.sp. *cudenis*), this phytopathogen can attack different species of palm trees (Araceae family plants), such as the oil palm tree (f.sp. *elaeidis*), the date palm (f.sp. *albedinis*) as well as decorative species (f.sp. *canariensis* and *palmarum*).[6-7]

Once the infection is initiated by *F. oxysporum* on plants, the regulation of this pathogen is difficult to handle. Indeed, the contamination of soils by *F. oxysporum* implies severe treatments to avoid its dissemination. Most often, a chemical treatment is carried out, rending the soil sterile and noncultivable for several seasons.[8-10] The pathogenicity is due to fungal progression into vascular tissue, which may elicit an immediate host response, successfully restricting the invader; an otherwise ineffective or delayed response reduces the vital water-conducting capacity and induces wilting.[11] On the other hand, the plant might be able to tolerate limited fungal growth within xylem vessels provided that it was initially colonized by an endophyte.[12] In this case, any further changes in the host or parasite could disturb the relationship in a way that fungal activities or a host response would induce disease symptoms.

Faced with these infections, *F. oxysporum* biocontrol approaches have been investigated, showing the beneficial impact of environmental microorganisms in defense of the plant against this phytopathogen. Jie *et al.* suggested the preponderant role of the endophytic community in the regulation of *F. oxysporum.*[13]

Endophytes are microorganisms living over a period of their life cycle between plant cells without causing apparent damage. Specialized metabolites from plant endophytes, such as peptides or ergosterol derivatives, showed antagonist activity against phytopathogens, including *F. oxysporum.*[14-17] Although endophytes seem to be possible research resources for anti-phytopathogen compounds, the major difficulty in natural product research is the isolation of already known compounds during the study of active strains. As an example, it has been estimated that only 10-15% of the biosynthetic capacity of actinomycetes and fungi is expressed under standard laboratory conditions.[18] Most secondary pathways are silent due to the absence of natural living conditions when a pure strain is cultured on synthetic standard media. These silent pathways can be turned on by different stimuli: agitation, pH, temperature, the addition of enzyme inhibitors, or dual cultures, for example. Bode *et al.* defined the term OSMAC (one strain many compounds) to designate that one strain could potentially provide different metabolite profiles depending on the culture parameters.[19-20] By expending the biosynthetic potential of strains, their chemical diversity and thus the probability of discovering original metabolites are increased. In the same vein, new metabolites can be efficiently isolated from cocultures because biotic stress mimed with cocultures can induce chemical defense metabolites such as antimicrobial compounds.[21-22]

In this study, a collection of 197 endophytes isolated from the leaflets of the palm tree *Astrocaryum sciophilum* (Miq.) Pulle growing in the understory part of Amazonian forest[23] was screened by a confrontation test against the phytopathogen *F. oxysporum* f. sp. *ciceris* and *F. oxysporum* f.sp. *albedinis*. *A. sciophilum* is a large undergrowth palm in the Asteraceae family

from the primary forests of French Guiana. In this Asteraceae, the stems of young plants are generally underground, but in older plants, they grow more above the ground.[24] Its small size in tropical forests makes it a receptor for plant matter from surrounding trees that traps between its leaves. This palm is thus in contact with the ground but is also very exposed to phytopathogenic microorganisms from the environment.[25] Consequently, it can be affected by pathogens of the *Fusarium* genus in the same way as other Asteraceae. However, it presents great longevity (age of maturation estimated at 170 ± 70 years), and it is found in all undergrowths of South American primary forests; this ecological success may be due to symbiosis with competitive endophytes. Two endophytic strains were selected based on activity, and their chemical diversity was explored to identify active specialized metabolites. Time-dependent production of these chemical compounds was studied by matrix-assisted laser desorption/ionization coupled to time-of-flight (MALDI-TOF) imaging.[26,27] The methodological approach of this study and details of the experimental procedures are summarized in scheme 1.

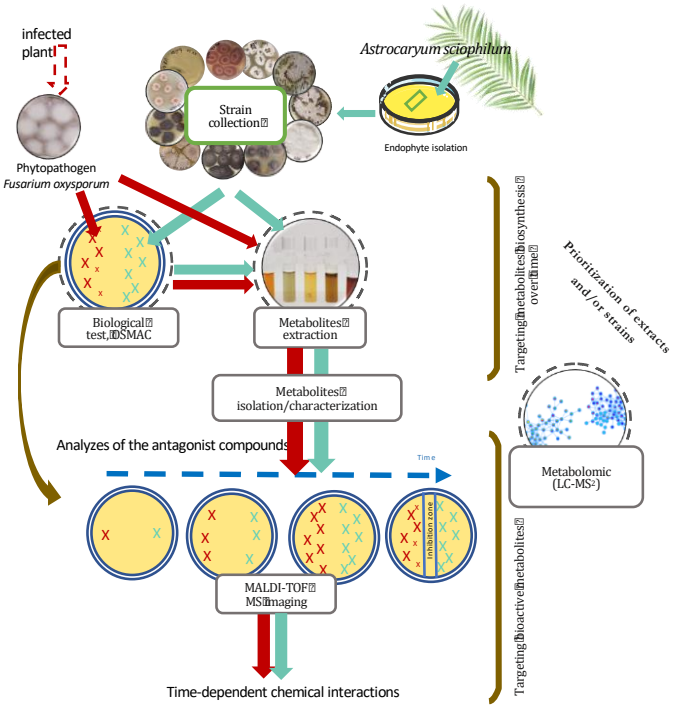

Scheme 1. Diagram of the methodological approach for the analysis of antagonistic compounds produced during endophyte/phytopathogen interspecies confrontation.

MATERALS AND METHODES

General Experimental Procedures. Optical rotations were measured using an Anton Paar MCP 300 polarimeter in a 350 µL cell with a length of 100 mm. UV spectra were recorded in acetonitrile using a PerkinElmer Lambda 5 spectrophotometer. Specific rotation was obtained in $CHCl_3$ with a JASCO P-1010 polarimeter. IR spectra were obtained on a Nicolet FTIR 205 spectrophotometer. Circular dichroism spectra were acquired on a Jasco® J-810 spectropolarimeter in a 1 cm cell at 20°C and treated with the SpectroManager® software. NMR spectra were recorded in CD_3OD or CD_3CN on a Bruker 500 MHz spectrometer or a Bruker 600 MHz spectrometer equipped with a 2 mm invers detection probe. Chemical shifts (δ) are reported in ppm based on TMS signal. Coupling constants (*J*) are in hertz. High-Resolution ElectroSpray Ionization-TOF MS in positive mode (HRESI-TOF) measurements were performed using a Waters Acquity UPLC system with column bypass coupled to a Waters Micromass LCT Premier time-of-flight mass spectrometer equipped with an electrospray interface (ESI). All solvents were HPLC grade and HPLC-grade water was obtained with a Milli-Q water purification system (Synergy, Merck).

Isolation and identification of endophytes. Leaflets of *A. sciophilum* palms were sampled in French Guiana in "Piste de Saint-Elie", Sinnamary, in July 2014. The general procedures adopted for isolation of the microorganisms followed the methodology described by Weber *et al*. with few modifications.[28] After collection, plant materials were washed with sterile water and surface-sterilized by sequential immersion in 70% aqueous ethanol (3 min), followed by 5% aqueous sodium hypochlorite (5 min) and finally by 70% aqueous ethanol (1 min). Leaves were cut into small pieces (1−0.5 cm^2) which were placed on Potato Dextrose Agar medium (PDA, Fluka Analytical, Germany) in Petri dishes at 28°C (4−5 parts per Petri dishes). The leaf fragments were cultured for a maximum of 1 month. A total of 197 endophytes (131 fungal isolates and 66 bacterial isolates) was purified by repeating culturing on fresh media. All the

isolated strains were deposited in the « ICSN/CNRS Strain library France ». The strains are maintained in at -80 °C.

For molecular identification of the isolated endophytes, PCR primers were used to amplify and sequence 16S rDNA and ITS region for bacteria and fungi respectively. BLASTs matching were carried out with the obtained sequences. Sequences were aligned in MAFFT version 7 (https://mafft.cbrc.jp/alignment/server/) and phylogenetic trees were obtained using CIPRES (https://www.phylo.org). Sequences have been deposited on GenBank (https://www.ncbi.nlm.nih.gov/nuccore/?term=Astrocaryum+sciophilum%2C+Barth%C3%A9lemy). The sequence of BSNB-0294 was registered in the NCBI GenBank database with the accession number MK650343; BSNB-0299 under number MK650346.

Detection of antifungal activity against *F. oxysporum* f.sp. *ciceris*

Biological material. F. oxysporum f.sp. *ciceris* was provide by Agroscope of Geneva and *F. oxysporum* f.sp. *albedinis* was purchased from Brest University under voucher UBOCC-A-101158.

Co-culture. To identify the antifungal activity of the isolated endophytes, each endophyte and *F. oxysporum* f.sp. *ciceris* were allowed to grow in close proximity on PDA up to five weeks at 28°C. Co-cultures were observed weekly to identify inhibition halos of the growth of *F. oxysporum* f.sp. *ciceris*. For the active isolate, volatile organic compounds (VOCs) with antifungal activity were detected by culturing the endophyte and the phytopathogen on two different PDA plates and sealing them together. Physical contact between the two strains was then avoided.

Antibiograms. Antibiograms were performed with the ethyl acetate extract and compounds **2** to **8**. 30 µL at the concentrations of 1 (compounds **3**, **4** and **6**), 5 (compounds **2**, **5** and **7**) and 50 mg/mL (compound **8**) were deposited on Antibiotic trial paper 6 mm diameter (D. Dutscher, Brumath). The diffusion discs were placed on Petri dishes where the phytopathogen was sown,

and left at 28°C for 3 days. Clotrimazole (23593-75-1, Sigma) was used at positive control at 0.5 µM and dimethyl sulfoxide (DMSO) served as negative control.

Agar diffusion assays. To test the antifungal activity of endophyte's extract or metabolites, agar diffusion assays were undertaken (n=3 replicates). Samples (50 µL at 10 or 5 mg/mL) were putted in a well at the middle of the PDA plate. Crude extract and fraction 5 as well as Xylariacein A and B were tested against *F. oxysporum* f.sp. *ciceris* by depositing 50 µL of a 5 mg/mL and/or 10 mg/mL of solutions. It was observed the inhibition of FOCIC growth when halos were formed on the surface of the agar around the deposit. Clotrinazole has been used as positive control. Phytopathogen was growth around the sample at 28°C during 3-5 days. Clotrimazole (23593-75-1, Sigma) was used at positive control at 10 mg/mL and dimethyl sulfoxide (DMSO) served as negative control.

Antimicrobial activities. Antimicrobial activity was tested on Methicillin-resistant *Staphylococcus aureus* ATCC 33591 and a clinical strain of *Trychophyton rubrum* (purchased from the Pasteur Institute). Crude extracts, fractions and molecules were tested according to the reference protocol of the European Committee on Antimicrobial Susceptibility Testing (EUCAST, http://www.eucast.org, 11 April 2016).[29] The standard microdilution test as described by the Clinical and Laboratory Standards Institute guidelines (M7, M27 and M38) was used to determine minimal inhibition concentrations (MIC) against dermatophyte fungi, bacteria, and yeasts. Crude extracts and pure compounds were tested at concentrations ranging from 256 to 0.5 µg/mL. The microplates were incubated at 35°C. MIC values were obtained after 24 h for bacteria, 48 h for yeasts and 5 days for fungi. All assays were conducted in duplicate.

Cytotoxic activity measurement. MRC-5 human embryonal lung fibroblast cell line (ATCC CCL-171). As previously described by Tempête *et al.*[30] the cells were cultured in Eagle's Minimal Essential Medium (EMEM, containing 4.5 g/L of glucose) supplemented with a non-

essential amino acid mixture, a selection of vitamins and 10% heat-inactivated fetal bovine serum. The cell lines were incubated at 37 °C, in a 5% CO_2, 95% air atmosphere. Crude extract for each strain was tested at 10 µg/ml. Docetaxel (Sigma-Aldrich, France) was used as positive control.

UHPLC analysis

Cultivation and extraction of secondary metabolites. Mono- or co-cultures were conducted at 28°C in 10 Petri dishes (10 cm diameter) of PDA media. Then, plates or selective parts of the plates were extracted with ethyl acetate (EtOAc) at room temperature during 24h. The organic phase was removed via filtration, washed three times with H_2O, dried with anhydrous solid Na_2SO_4 and evaporated using a rotary evaporator under reduced pressure to yield a crude mixture.

UHPLC-UV analysis. Extracts were analysed using a Shimadzu® system fitted with an analytical column (Kinetex® C18, 2.1 x 150 mm, 1.7 µm) and coupled with ELSD SEDEX LT90 (SEDERE®) and a UV detector SPD-M30A (Shimadzu®). A water-acetonitrile gradient from 5-100% of acetonitrile was conducted in 7 minutes at 0.6 mL/min. Both water and acetonitrile were acidified with 0.1% formic acid. 20 µL of extracts were injected at 1 mg/mL in methanol.

UHPLC-MS/MS and data analysis. UHPLC-HRMS/MS analyses were performed on a Dionex Ultimate 3000 RSLC system fitted with a ThermoScientific Accucore C18 column (2.1 x 100mm, 2.6µm) and coupled to an Agilent 6540 Q-TOF mass spectrometer (Agilent Technologies) using a heated electrospray ionization source. The mass spectrometer parameters were as follows: source voltage, 3.5 kV (positive ion mode); sheath gas flow rate (N_2), 7 L/min; nebulizer pressure, 30 psi; spare gas flow rate, 10 L/min; capillary temperature, 325 °C; skimmer voltage, 45 V; fragmentor voltage, 150 V; nozzle voltage, 500 V. The data-dependent MS/MS events were performed on the five most intense ions detected in full scan MS. The

MS/MS isolation window width was 1.3 arbitrary units, and the collision energy was set to 35 eV. In data-dependent MS/MS experiments, full scans were acquired at a resolution of 20 000 at *m/z* 922. 5 µL of each extract were injected at a concentration of 1 mg/mL. The linear gradient between acetonitrile and water (0.1% formic acid modifier) was made from 20% to 100% of acetonitrile over 20 min following by a plateau at 100% acetonitrile during 3 min. Internal calibration was performed using a mixture of purine (*m/z* 121.0509 $C_5H_4N_4$) and HP-921 (*m/z* 922.0098 $C_{18}H_{18}O_6N_3P_3F_4$).

MZmine 2 Data-Preprocessing Parameters. Raw.d files were converted into mzXML files using MSConvert software. Then mzXML files were processed using MZmine 2.37.[31] Mass detection was realized with centroid mass detector with the noise level set to 1.0E2 for MS level set to all. The ADAP chromatogram builder[32] was achieved using a minimum group size of scans of 5, minimum group intensity threshold of 1.0E2, minimum highest intensity of 1.0E2 and m/z tolerance of 0.005 or 10.0 ppm. Wavelets (Automated Data Analysis Pipeline) algorithm was used for chromatogram deconvolution with the following settings: S/N threshold of 100, intensity window SN, minimum feature height of 1000, coefficient area threshold of 10, peak duration range between 0.01 and 2.0 and the RT wavelet range between 0.0 and 0.05. The *m*/*z* and RT range for MS/MS scan pairing was set to 0.008 Da and 0.3 min respectively. Chromatograms were deisotoped using the isotopic peaks grouper algorithm with a *m*/*z* tolerance of 0.003 (5 ppm), a RT tolerance of 0.1 (absolute), a maximum charge of 1 and the representative isotope used was the most intense. Peak alignment was performed using the join aligner method: m/z tolerance of 0.005 or 10.0 ppm, weight for *m*/*z* of 0.003, RT tolerance of 0.5 min, weight for RT of 0.3. Peak list was exported as a mgf file. Row ID, row *m*/*z*, row retention time and peak area was also exported in an associated CSV file.

Molecular Network Analysis. After the preprocessing of the LC-MS/MS data with MZmine 2.37, the mgf file was then processed with MetGem 1.3.4 software[33] to calculate and visualize

the Molecular Network (MN). MN was generated using the following parameters: *m*/*z* tolerance set to 0.02, minimum matched peaks set to 6, topK set to 10, minimal cosine score value (CSV) of 0.7 and Max. Connected component size of 100. Associated CSV file was then loaded. For the mapping process, relative quantification of each ion was represented as pie chart-diagrams, whose proportions were based on respective areas of the corresponding extracted ion chromatograph area (EIC). The spectra in the network were then searched for analogues against the spectral libraries available. The library spectra were filtered in the same manner as the input data. All matches kept between network spectra and library spectra were required to have a score above 0.7 and at least 6 matched peaks. The m/z tolerance for the search of analogues was set to 100. For a more advanced retreatment of the network, MN was also exported on Cytoscape 3.7.0 software.

Metabolites extraction, fractionation, isolation and identification

Large-scale cultivation of the co-culture and metabolite extraction. BSNB-0294 and *F. oxysporum* f.sp. *ciceris* were co-cultivated 21 days at 28°C on 330 x14 cm Petri dishes of PDA media. Each strain was separately extracted three times consecutively with ethyl acetate (EtOAc) at room temperature. Organic solution was washed as previously described for UHPLC analyses. Crude extracts of BSNB-0294 isolate and *F. oxysporum* f.sp. *ciceris* (FOCIC) yielded 3.53 g and 2.63 g, respectively.

Crude extract fractionation. Flash chromatography were performed on a Grace Reveleris system equipped with a 120 g C_{18} column. Flow rate was fixed at 80 mL/min and detection was performed with dual UV at 210 and 270 nm and ELSD. Elution was made with a 5 min step-gradient between water and acetonitrile acidified with 0.1% formic acid: v/v, 95:5, 75:25, 50:50, 20:80 et 0:100. All the data related to the fractionation of BSNB-0294 and FOCIC extracts as well as the isolation and the characterization of the compounds are indicated in the SI.

MALDI-TOF analyses

Sample preparation for mass spectrometry imaging. To follow an evolution of co-culture in a time course, 10 PDA petri dishes were inoculated at day 0 with one suspension of BSNB-0294 and one of *F. oxysporum* f.sp. *ciceris*. Suspensions were initially prepared in water, then 10 µL of each suspension were dropped at the same spot for all plates. Fingerprints of the co-culture were obtained at days 3, 4, 5, 6, 7, 10 and 23.

Mass spectrometry imaging. MALDI-TOF MS analyses were performed using an UltrafleXtreme mass spectrometer (Bruker Daltonics, Wissembourg, France). Pixel size was set at 90µm with 500 laser shots per pixel. Acquisitions were performed in positive ion mode in the *m/z* 140−1700 range (LaserPower = 87%; SmartBeam Size = Large; Laser Frequency = 2000 Hz). Mass calibration was carried out using a mixture of peptides (Pepmix 5, LaserBioLabs, Nice, France). Data were processed using FlexAnalysis 3.4 and FlexImaging 4.1 (Bruker Daltonics, Bremen) software. To afford the MALDI-TOF imaging of the co-culture between BSNB-0294 and *F. oxysporum* f.sp. *ciceris*, an ITO-coated glass slide was pressed on the co-culture to transfer the metabolites. The glass slide was dried in desiccator for 15 min. Matrix (CHCA, Sigma-Aldrich, at 10 mg/mL in 70% acetonitrile acidified with 0.1% TFA) was deposited by pulverisation with a TM-Sprayer (HTX Imaging) using an ethanol flow rate of 0.24 mL/min, a nebulized nitrogen pressure of 10 psi and a nebulizer temperature at 75°C.

RESULTS

Antagonism between endophytes and *F. oxysporum.* All endophytes isolated from leaflets of *Astrocaryum sciophilum* palms were identified through DNA extraction, amplification, and sequencing using a universal DNA marker ribosomal cluster. Most fungal strains were related to Xylariaceae based on the closest ITS sequences in NCBI (BLAST similarity). Indeed, our collection contained 68% fungi, and 17% of them were identified as being part of the Xylariaceae family.[34] All strains of our collection were tested for their capacity to inhibit the growth of the phytopathogen *F. oxysporum* (f.sp. *ciceris* and f.sp. *albedinis*).

Fungi BSNB-0299 and BSNB-0294 belonging to the Xylariaceae family exhibited inhibited growth of phytopathogens over a period of five weeks of culture (Figures S1).

The strain BSNB-0299 was identified as *Muscodor* sp. To determine if the inhibitions observed are due to VOCs as already described in the *Muscodor* genus, BSNB-0294 and -0299 strains were tested on the phytopathogen in a "face-to-face" culture.[35] Inhibition was observed for BSNB-0299 but not for BSNB-0294 (Figure S2), confirming that VOCs might be involved in *Muscodor* sp. BSNB-0299 activity. Since inhibition of *F. oxysporum* growth by BSNB-0294 was due to metabolites diffused in the culture media, this latter strain was chosen for further chemical analysis.

Molecular network analysis of endophyte and *F. oxysporum* extracts over time during competition. A study was then undertaken to determine when the molecules inducing phytopathogen inhibition are biosynthesized. To reach this goal, dual cultures of BSNB-0294 and *F. oxysporum* f.sp. *ciceris* or f.sp. *albedinis* were prepared, and extracts of each fungus were achieved with ethyl acetate after one, two, or three weeks of competition. The extracts were analyzed by ultrahigh-performance liquid chromatography coupled to ultraviolet detection (UHPLC-UV) at 254 nm. Analysis of BSNB-0294 extracts showed that some molecular signals increased over competition time and were not detected in the monoculture extract of the endophyte. Elicitation of specialized metabolites when competition is occurring was also obtained for phytopathogen extracts. This trend seems to be more pronounced in *F. oxysporum* f.sp. *ciceris* (FOCIC) than in f.sp. *albedinis* (Figures S3). Therefore, we focused on the specialized metabolome of the FOCIC phytopathogen.

Afterwards, BSNB-0294 and FOCIC EtOAc extracts were analyzed by UHPLC coupled to high-resolution tandem mass spectrometry (UHPLC-HRMS/MS) using the data-dependent acquisition (DDA) mode. Data were first processed by MZmine 2.37, and molecular networks were generated and visualized by MetGem software.[33,36] Relative quantification of the ion

signals was depicted using pie chart diagrams, with their proportions based on the respective areas calculated from the corresponding extracted ion chromatograph (XIC). T-SNE representation was adopted because it preserves the interactions between related groups of tandem mass spectra. The resulting molecular network grouped 1176 nodes (Figure 1 and S4). Mapping of experimental conditions, *i.e.*, taxonomy and days of coculture, was applied by attributing a given color code to each condition. Using the database query algorithm included in MetGem software, several clusters were annotated. For example, two clusters a and b were related to singly and doubly charged cyclopeptides corresponding to enniatin and beauvericin analogs. This analysis confirmed that some compounds produced by the endophyte diffused in the culture medium are distributed during coculture at the phytopathogen level. The same phenomenon was also observed between compounds produced by the phytopathogens.

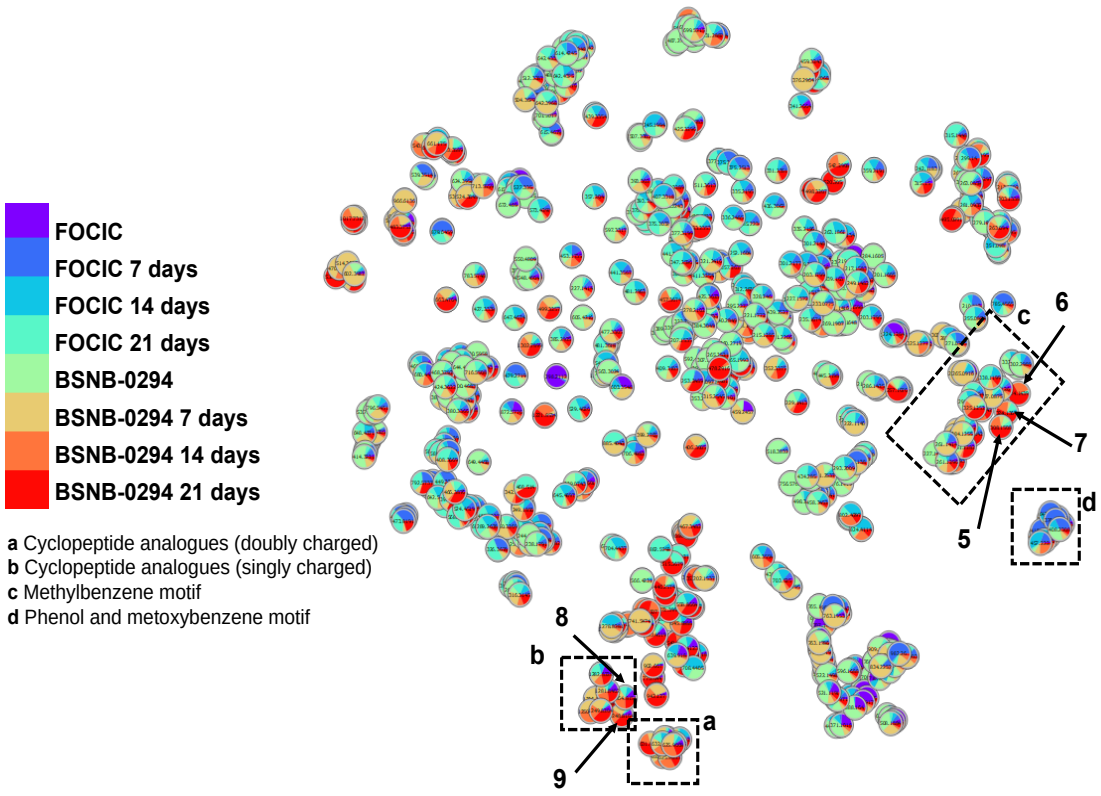

Figure 1. T-SNE representation of the molecular network grouping MS/MS data from extracts of *F. oxysporum* f.sp. *ciceris* (FOCIC) and Xylariaceae sp. (BSNB-0294) in culture alone or in coculture after one, two, and three weeks.

Isolation of the metabolites produced in the BSNB-0294 extract. An EtOAc extract of the zone where BSNB-0294 grew in confrontation with FOCICs (at 21 days of coculture) was

obtained and led to the isolation of two known compounds: (+)-(4*S*)-4,8-dihydroxy-α-tetralone (**1**), iminophenylpropanamide (**2**) and an analog of iminophenylpropanoic acid (**3**) together with 6 new metabolites **4**–**9** (Figure 2).

Compound **1** was identified as the naphthalenone derivative (+)-(4*S*)-4,8-dihydroxy-α-tetralone or (4*S*)-isosclerone by comparison with literature data. The absolute configuration was determined by comparison with a previously published optical rotation value.[37]

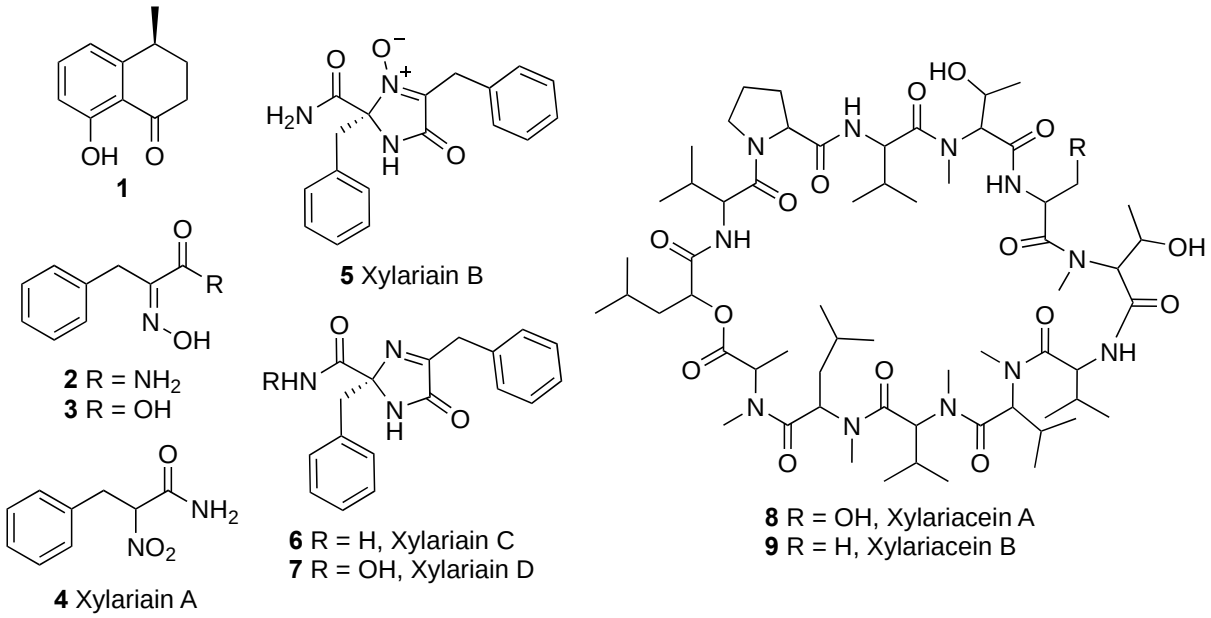

Figure 2. Structures of metabolites isolated from the BSNB-0294 endophyte after confrontation experiments against FOCICs.

Compound **2** showed a pseudomolecular ion at *m/z* 179.0816 corresponding to the molecular formula $C_9H_{10}N_2O_2$ (calc. $[M+H]^+$ 179.0815, err. 0.56 ppm). The ^{1}H-NMR spectrum as well as the ^{1}H-^{13}C correlation in the HSQC spectrum allowed the identification of a phenyl ring (δ_H 7.26-7.19 and δ_C 129.8, 129.4 and 127.2), a methylene (δ_H 3.87 and δ_C 29.5) and three exchangeable protons (δ_H 9.58, 6.71 and 5.74). The ^{13}C-NMR spectrum indicated the presence of three nonprotonated carbons. One belonged to the phenyl moiety (δ_C 138.0), and the two others were at 153.6 and 165.9 ppm. The ^{1}H-^{13}C correlations in the HMBC spectrum linked the methylene moiety to the phenyl ring (Table S1 and Figure S13). This methylene also correlated with both nonprotonated carbons at δ_C 153.6 and 165.9. The ^{1}H-^{15}N correlation in the HSQC

spectrum led to identifying an NH_2 group at δ_N 92.0, and the HMBC spectrum ^1H-^{15}N showed a correlation between the methylene protons and a second nitrogen at δ_N 373.5, which coincides with the displacement of an aromatic amine or a nitro group. To respect the calculated chemical formula, the quaternary carbon at δ_C 165.9 corresponds to a C=O double bond, and a hydroxyl must be present on the molecule (Table 1). (*E*)-2-(Hydroxyimino)-3-phenylpropanamide (**2**) with the presence of an oxime was then identified, satisfying all the observed correlations and the chemical shifts of protons, carbons, and nitrogen. The (*E*) configuration was determined by comparison with literature data.[38]

Compound **3** showed a pseudomolecular ion at *m/z* 180.0659, corresponding to the molecular formula $C_9H_9NO_3$ (calc. $[M+H]^+$ 180.0655, err. 2.22 ppm). The ^1H and ^{13}C NMR spectra are identical to those of compound **2** except for the exchangeable protons, including a proton at δ_H 10.01 (Table 1). The ^1H-^{15}N in HSQC and HMBC spectra show no correlations. Compared to molecule **2**, the amide functional group is replaced by carboxylic acid (Table 2). Therefore, compound **3** was identified as (*E*)-2-hydroxyimino-3-phenylpropanoic acid by comparison of the NMR data in the literature.[39]

Molecule **4** showed a pseudomolecular ion at *m/z* 195.0772, leading to the molecular formula $C_9H_{10}N_2O_3$ (calc. $[M+H]^+$ 195.0764, err. 4.10 ppm). The ^1H-NMR spectrum and the ^1H-^{13}C correlation observed in the HSQC spectrum allow the identification of a phenyl ring (δ_H 7.25-7.21 and δ_C 130.0, 129.7 and 128.3), one methylene (δ_H 3.41/3.29 and δ_C 36.7) and two exchangeable protons (δ_H 6.49 and 6.07, Table 1). A methine is also identified (δ_H 5.35 and δC 90.5). Again, an unsubstituted NH_2 of the amide group at δ_N 103.5 was identified by the ^1H-^{15}N correlation in the HSQC spectrum, and the second nitrogen predicted by the chemical formula was not protonated (Table 1). According to the COSY ^1H-^1H correlations, methine H-3 and methylene H-4 are placed next to this nonprotonated nitrogen (Figure 3). In the same way as for molecule **2**, the phenyl ring was placed next to methylene. The HMBC spectrum showed

^{1}H-^{15}N correlations between the H-3 and H-4 protons and the nonprotonated nitrogen at δ_N 79.8; this nitrogen was thus placed in position 3. An amide function was identified, making it possible to satisfy the ^{1}H-^{13}C correlations in HMBC between H-3, H-4, and δ_C 166.0. Two oxygens remained to be placed to respect the chemical formula $C_9H_{10}N_2O_3$. The nonprotonated nitrogen was therefore identified as the center of a nitro group. The upfield displacement of δ_N 79.8 compared to usual nitro groups, usually approximately 300 ppm, can be explained by the existence of a cone shielding anisotropy generated by the vicinal phenyl moiety. In addition, an ion signal at *m/z* 148.0750 was observed in the MS spectrum, which corresponded to the loss of HNO_2 from the protonated molecular ion (th -47.0007 amu; exp -47.0014 amu). The presence of a nitro group was also confirmed by the two typical absorbance bands at 1570 and 1330 cm^{-1} in the IR spectrum (Figure S32). This new compound is 2-nitro-3-phenylpropanamide (**3**) and was named xylariain A.

Table 1. ^{1}H, ^{13}C and ^{15}N NMR Spectroscopic Data of **2**–**4**

	2			**3**		**4**		
Position	δc	δ_N	δ_H (*J* in Hz)	δc	δ_H (*J* in Hz)	δc	δ_N	δ_H (*J* in Hz)
1		92.2	6.71 s 5.74 s				103.5	6.49 (1H, br s) 6.07 (1H, br s)
2	165.9			164.8		166.0		
3	153.6			151.7		90.5		5.35 dd (8.6, 6.7)
4	29.5		3.87 s	30.6	3.88 s	36.7		3.41 dd (14.2, 8.6)
5	138.0			137.4		136.1		3.29 dd (14.2, 6.7)
6/10	129.8		7.26 m	129.7	7.28 m	130.0		7.21m
7/9	129.4		7.26 m	129.5	7.29 m	129.7		7.25 m
8	127.2		7.20 m	127.4	7.21 m	128.3		7.21 m
11		373.5					79.8	

^{1}H NMR data recorded at 500 MHz in CD_3CN for **4** and **3**, at 600 MHz in CD_3CN for **2;** ^{13}C NMR data recorded at 125 MHz in CD_3CN for **3** and **4**, at 150 MHz in CD_3CN for **2** and ^{15}N data recorded at 50 MHz in CD_3CN for **3** and **4**, at 60 MHz in CD_3CN for **2.**

The molecular formula $C_{18}H_{17}N_3O_3$ of compound **5** was deduced from the protonated molecular ion at *m/z* 324.1345 (calc. $[M+H]^+$ 324.1343, err. 0.62 ppm). ^{1}H-^{13}C correlations observed in the HMBC spectrum confirmed the presence of two benzyl subunits (Table 2). Protons from one methylene correlated with two nonprotonated carbons at δ_C 139.5 and 164.0, and protons from the second methylene correlated with two other nonprotonated carbons at δ_C

88.9 and 166.8 (Table 2). The ^{1}H-^{15}N HSQC spectrum indicated the existence of two amide nitrogens at δ_N 96.7 and 113.9 and one downfield nitrogen at δ_N 304.7 (Figure 3 and S40). A ^{1}H-^{15}N HMBC correlation was observed between H-4' and the nitrogens at δ_N 113.9 and 304.7, while proton 4 correlated with the downfield nitrogen only. The analytical data turned out to be consistent with the presence of an aminal in C-3 in which the deshielded nitrogen is oxidized to form an imine *N*-oxide derivative. The proposed structure, corresponding to 2,4-dibenzyl-2-carbamoyl-5-oxo-2,5-dihydro-1*H*-imidazole-3-oxide, was also confirmed by the IR data. This molecule was named xylariain B.

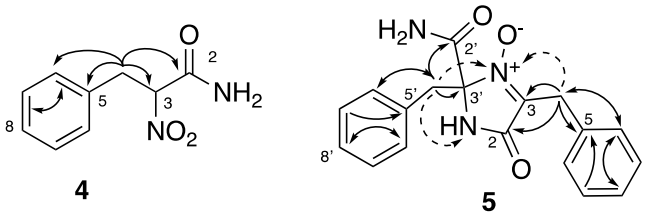

Figure 3. ^{1}H-^{13}C HMBC correlations (plain arrows) ^{1}H-^{15}N HMBC correlation (dashed arrows)

The molecular formula $C_{18}H_{17}N_3O_2$ of compound **6** was deduced from its protonated molecular ion at *m/z* 308.1407 (calc. $[M+H]^+$ 308.1394, err. 4.21 ppm). ^{1}H and ^{13}C spectra are similar to those of compound **5** (Table 2), although in **6**, ^{1}H-^{15}N HSQC and HMBC spectra showed three nitrogens at δ_N 99.5, 136.0, and 136.7. The similarity of the NMR data set, as well as the very strong upfield shift of the imine nitrogen, indicated that this compound was not an *N*-oxide. This also accounts for the chemical shift variation for C-3 and C-4 in compound **6**. In **5**, the *N*-oxide mesomeric effect is enriched in electrons at position 3. Overall, compound **6** was identified as 2,4-dibenzyl-5-oxo-2,5-dihydro-1*H*-imidazole-2-carboxamide and was named xylariain C.

Compound **7** is an isomer of compound **5** based on the ESI-HRMS data showing a protonated molecular ion at *m/z* 324.1342 (calc. for $C_{18}H_{18}N_3O_3^+$: $[M+H]^+$ 324.1343, err. -0.31 ppm). 1D and 2D NMR spectra were similar to those of compound **6**. The relative shielding of C-2' and the absence of compound **6** N-1' protons at δ_H 6.11 and 6.39 indicated that nitrogen N-

1' was hydroxylated and not N-11, as in compound **5** (Table 2). Compound **7** was then 2,4-dibenzyl-*N*-hydroxy-5-oxo-2,5-dihydro-1*H*-imidazole-2-carboxamide and was named xylariain D.

Clearly, these three metabolites are dimeric phenylalanine derivatives. Nonetheless, the absolute configuration of the phenylalanine α carbon does not necessarily dictate the absolute configuration in C-3' in **5**–**7** because this position is oxidized upon formation of the aminal moiety. Configurations of compounds **5**–**7** were obtained by comparison of the theoretical and experimental ECD spectra (Figures S57-S58). Experimental electronic circular dichroism spectra recorded in acetonitrile showed three positive absorption bands at 220, 250, and 290 nm, allowing us to assume the *R* configuration of C-3' (Figure S57-S58).

Table 2. ^{1}H, ^{13}C, and ^{15}N NMR Spectroscopic Data of **5**–**7**

	5			**6**			**7**	
Position	δc	δ_N	δ_H (*J* in Hz)	δc	δ_N	δ_H (*J* in Hz)	δc	δ_H (*J* in Hz)
1		113.9	7.79 s		136.0	8.26 s		8.25 s
2	164.0			171.1			171.6	
3	139.5			165.4			165.3	
4	28.4		3.68 d (14.6)	34.9		3.69 d (15.7)	34.9	3.68 s
			3.54 d (14.6)			3.66 d (15.8)		
5	135.4			136.3			136.2	
6/10	129.5		6.92 m	130.1		7.04 m	130.2	7.04 m
7/9	129.6		7.20 m	129.4		7.28 m	129.4	7.26 m
8	127.8		7.20 m	127.6		7.24 m	127.6	7.23 m
11		304.7			136.7			
1′		96.7	7.50 br s		89.5	6.39 br s		n.d.
			6.34 br s			6.11 br s		
2′	166.8			170.8			166.1	
3′	88.9			87.4			86.8	
4′	41.5		3.59 d (14.4)	43.0		3.42 d (13.8)	43.0	3.41 d (13.5)
			3.31 d (14.4)			3.27 d (13.8)		3.28 d (13.5)
5′	132.3			134.2			133.9	
6′/10′	131.3		7.06 m	132.0		7.05 m	132.0	7.03 m
7′/9′	129.2		7.10 m	128.8		7.19 m	128.8	7.18 m
8′	128.7		7.20 m	128.0		7.22 m	128.0	7.21 m

^{1}H NMR data recorded at 500 MHz in CD_3CN for **5** and **7**, at 600 MHz in CD_3CN for **6;** ^{13}C NMR data recorded at 125 MHz in CD_3CN for **5** and **7**, at 150 MHz in CD_3CN for **6** and ^{15}N data recorded at 50 MHz in CD_3CN for **5** and **7**, at 60 MHz in CD_3CN for **6**. n.d.: not detected.

Compound **8** showed a protonated molecular ion *m/z* 1264.8133 corresponding to the molecular formula $C_{62}H_{109}N_{11}O_{16}$ (calc. $[M+H]^+$ 1264.8127, err. -0.51 ppm). ^{1}H-NMR and the ^{1}H-^{13}C correlation in the HSQC experiment allowed us to identify different types of protons

(Table S7, Figure S59-S65). First, four broad – presumably exchangeable – protons were detected at δ_H 8.94/8.14/8.02 and 7.89 ppm displacements. The integration of the peaks also made it possible to identify six rather unshielded methyls at δ_H values of 3.14/3.11/3.04/2.91/2.90 and 2.79 with carbon chemical shifts at δ_C 31.5/36.0/40.4/31.6/32.7 and 29.4, respectively. In view of their chemical shifts, these methyls would be linked to nitrogen. Between δ_H 3.5 and 5.2, fifteen methine protons were identified with δ_C between 52.6 and 74.6. The carbon chemical shifts indicated proximity to oxygen or nitrogen. Similarly, a methylene at δ_H 3.95 and 3.74 with δ_C at 49.0 would be close to oxygen in view of its chemical shift. Finally, many methyls were identified in the region between δ_H 0.5 and 1.5, and several methine or methylene protons were also superimposed in the region from δ_H 1.0 to 2.8. The ^{1}H-^{1}H and ^{1}H-^{13}C correlations observed in the 2D NMR spectra of COSY and HMBC made it possible to identify twelve amino acid subunits, six of which had a methyl group on their nitrogen (one leucine, one alanine, two threonines, and two valines), five amino acids were unchanged (one proline, one serine, and three valines) and the last corresponded to leucic acid (also named 2-Hydroxyisocaproic acid (HICA)), where the leucine α-nitrogen has been replaced by an oxygen. This assumption was based on the α-carbon chemical shift at δ_C 74.6. The raw formula $C_{62}H_{109}N_{11}O_{16}$ was respected with this assignment. Oxygen-bound sp3 carbons of threonines and serine were at δ_C 62.7 and 67.9. Overall, this molecule was identified as a depsipeptide, the amino acid sequence of which remained to be determined. ^{1}H-^{13}C correlations in the HMBC spectrum allowed us to identify two distinct parts (Figure 4). Indeed, correlations appeared between the protons α and the two carbons of the C=O double bonds that surround them, between the methyl group born by nitrogens and the carbons of the C=O double bond of the next amino acid, or between the β protons of the amino acid and the carbon of the C=O double bond.

However, the sequence could be completed with long-range ^{1}H-^{13}C correlations because 4 α protons exhibited the same chemical shift at δ_H 4.94. Eventually, as two amino acid sequences were identified, the only possible proposition for ring closure led to compound **8**. The sequence was confirmed upon exploring the MS/MS fragmentation pattern (Figure 5). Indeed, specific fragments were detected at *m*/*z* 770.5040, 643.4037 and 530.3127, corroborating the presence of an *N*-methylleucine next to two *N*-methylvalines. The fragments at *m*/*z* 622.4174, 523.3490 and 426.2968 confirmed the valine/proline/valine sequence. This cyclic depsipeptide was named xylariacein A.

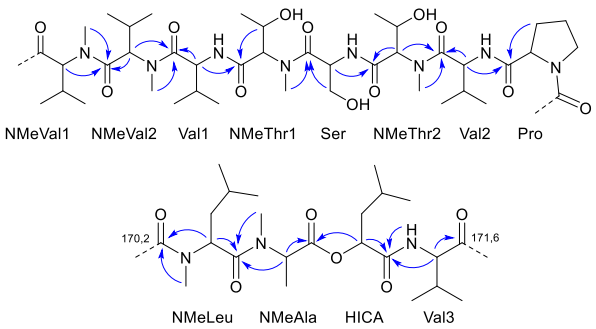

Figure 4. ^{1}H-^{13}C HMBC correlations giving amino acids sequence

Another depsipeptide compound (**9**) was isolated and showed an MS/MS spectrum very similar to that of xylariacein A. The predicted molecular formula was determined to be $C_{62}H_{109}N_{11}O_{15}$ (calc. $[M+H]^+$ 1248.8177, err. -1.92 ppm) indicated one loss of oxygen compared to (**8**). The differences in the ^{1}H-NMR spectrum were in the absence of the integrating signal for methylene from the serine at δ_H 3.82 and in a variation in the displacements of the protons of *N*-methylthreonine (NMeThr2): in place of the serine is an alanine with a methyl at δ_H 1.37. The fragmentation pattern was then analyzed to confirm this hypothesis (Figure S69) as for compound **8**. Depsipeptide **9** was named xylariacein B.

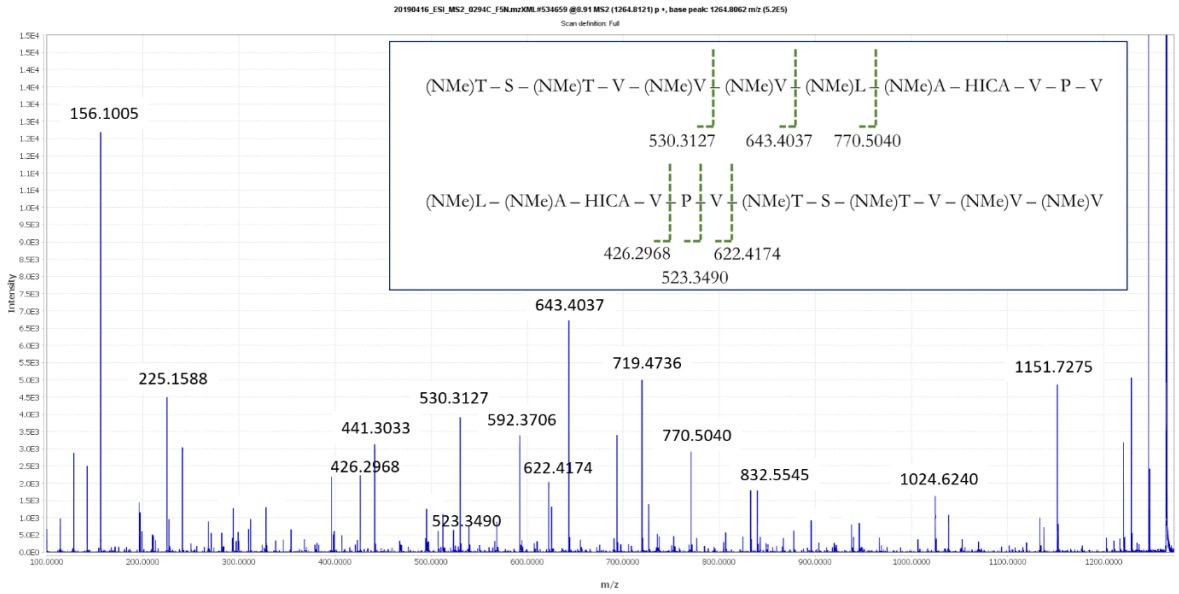

Figure 5. ESI-MS/MS spectrum of compound **8** at *m/z* 1264.8.

Isolation of the metabolites of F. oxysporum f.sp. ciceris (FOCIC). An EtOAc extract of FOCICs was also obtained from the 21-day coculture with BSNB-0294. Successive purifications of this extract by reverse-phase chromatography led to the isolation of four compounds: xylariacein A (**8**), bassiatin **(10)**, (–)-cyclonerodiol **(11)**, and the new compound **12** (Figure 6). The structures of the known compounds were determined by high-resolution mass spectrometry, NMR spectroscopy, and by comparison with the literature data.[40-41] Absolute configurations of bassiatin and (–)-cyclonerodiol were obtained according to optical rotation measurements.[42-43]

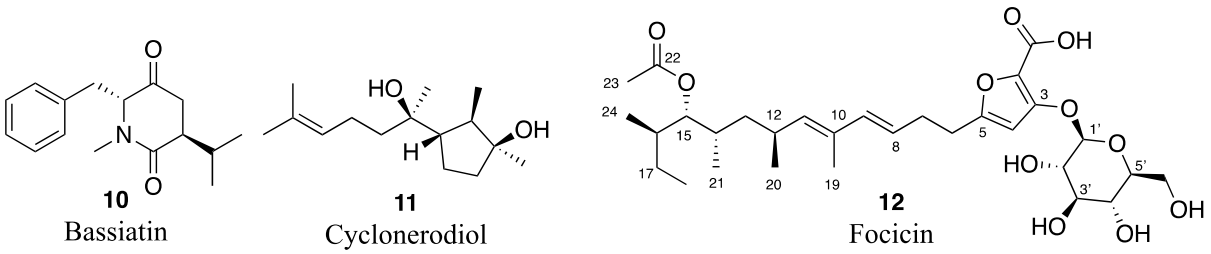

Figure 6. Structures of metabolites isolated from *F. oxysporum* f.sp. *ciceris* (FOCIC)

The molecular formula $C_{30}H_{46}O_{11}$ of compound **12** was deduced from the protonated molecular ion at *m/z* 583.3135 (ESI-HRMS, calc. $[M+H]^+$ 583.3113, err. 3.77 ppm). Examination of the ^1H spectrum and ^1H-^{13}C correlations in HSQC allowed the identification of 4 unsaturated (δ_H 6.09, 6.02, 5.56 and 5.20) and 9 saturated (δ_H 4.69, 4.65, 3.41, 3.39, 3.36,

3.28, 2.53, 1.85 and 1.69) methines, 5 methylenes (δ_H 3.80/3.70, 2.57, 2.43, 1.36/1.09 and 1.48/1.05) and 6 methyl groups. The ^{13}C NMR spectrum indicated the presence of six nonprotonated carbons (δ_C 173.1, 165.1, 164.2, 163.3, 132.6, and 123.7; Table 3). An alkyl chain was determined by the sequence of ^{1}H-^{1}H COSY cross-peaks from H-11 to H-18, and 3 methyls were placed at positions 12, 14, and 16. The chemical shift of C-15 at δ_C 83.7 ppm and the ^{1}H-^{13}C HMBC correlation between H-15 and a quaternary carbon C-22 at δ_C 173.1 indicated the presence of an ester on C-15 (Figure 7). An acetate group was placed at position 15 considering the HMBC correlation between H-23 and C-22. The H-6/H-7/H-8/H-9 sequence was determined based on COSY correlations. HMBC correlations of H-19/C-10, H-19/C-9, and H-19/C-11 indicated that the two alkyl chains were linked by a quaternary carbon at position 10 (δ_C 132.6) bearing a methyl group. The coupling constant between H-8 and H-9 was 15.4 Hz, which confirmed the *E* configuration of the C-8–C-9 double bond. ^{1}H-^{1}H NOE correlations between H-19/H-8 and H-9/H-11 allowed us to assign an *E* configuration for the second double bond. A pyranose moiety was deduced by the sequence of COSY cross-peaks for H-1'/H-2'/H-3'/H-4'/H-5' and H-6' along with the HMBC correlation H-1'/C-5' and the characteristic chemical shifts of carbons (anomeric proton at δ_C 106.3, methylene at δ_C 62.2 and methines at δ_C between 70 and 80). The NOESY correlation between H-1' (δ_H 4.69) and H-5' (δ_H 3.28) is consistent with a β-configuration. The NOESY spectrum also showed correlations between H-1' and H-3' and/or H-5'. The pyranose moiety was therefore defined as a β-glucoside. The presence of an oxygen atom can be deduced from the chemical shift of C-5. With respect to the predicted molecular formula, six quaternary carbons (δ_C 173.1, 165.1, 164.2, 163.3, 132.6, and 123.7), two oxygens, and one hydrogen remained to be placed. H-4 and H-1' had an HMBC correlation with carbon δ_C 123.7.

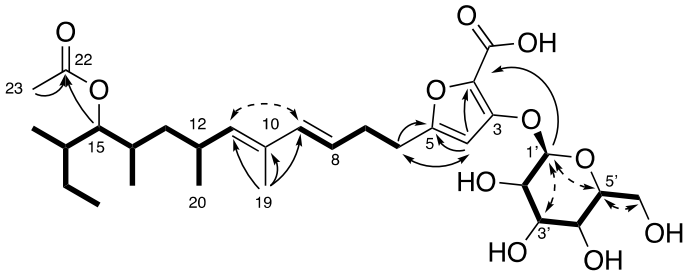

Figure 7. ^{1}H-^{13}C HMBC correlations (plain arrows), ^{1}H-^{1}H cosy correlations (bold lineaments) ^{1}H-^{1}H NOE correlation (dashed arrows)

A furan moiety substituted with the alkyl chain, glucose, and a carboxylic acid function suited to the molecular formula and the number of instaurations. The ^{1}H-^{13}C HMBC correlations between H-4, H-6, and C-5 allowed us to position the alkyl chain at position 5. The chemical shifts observed in ^{13}C NMR for C-5 (δ_C 163.3) and C-2 (δ_C 123.7) confirm the location of glucose at position 3 (Figure S81). The relative and absolute configurations were determined by ^{13}C NMR calculations on diastereoisomers in which the sugar moiety was defined as ß-D-glucose, the D configuration being by far the most common configuration found in nature.[44] One diastereoisomer was deduced to be correct with a 95% probability from the ^{13}C NMR chemical shift calculation based on the DP4 probability method (Figure S83).[45] Experimental electronic circular dichroism spectra were recorded in chloroform and compared to the calculated spectrum. A broad negative absorption band is observed at 290 nm, in agreement with the calculated spectrum for the 8*E*, 10*E*, 12*S*, 14*S*, 15*S*, 16*R* stereomers. Compound **12** was named Focicin.

Table 3. NMR spectroscopic data of **12** in CD_3OD at 500 (^{1}H) and 125 MHz (^{13}C)

Position	δ_H (*J* in Hz)	δ_C
1	-	165.1
2	-	123.7
3	-	164.2
4	6.01 s	103.1
5	-	163.3
6	2.59-2.55 m	34.4
7	2.43 td (10.7, 7.0)	31.2
8	5.56 dt (15.4, 7.0)	125.9
9	6.09 (1H, d, *J* = 15.4)	137.8
10	-	132.6
11	5.20 d (5.0)	139.3

12	2.53 m	31.4
13	1.36 m	39.9
	1.11-1.06 m	
14	1.85 m	33.3
15	4.65 dd (7.0, 5.7)	83.7
16	1.69 m	37.0
17	1.48 m	25.1
	1.05 m	
18	0.89 m	11.6
19	1.73 s	12.8
20	0.92 d (6.5)	20.3
21	0.88 m	17.6
22	-	173.1
23	2.05 s	20.9
24	0.87 m	16.0
1′	4.69 m	106.3
2′	3.41 m	75.1
3′	3.39 m	77.7
4′	3.36 m	70.8
5′	3.28 m	78.5
6′	3.80 dd (12.0, 2.2)	62.2
	3.70 dd (12.0, 5.0)	

Activity of the confrontation metabolites. Compounds **2** to **7** were tested in pure form and did not inhibit phytopathogen growth at the tested concentrations (50 µL at 10 and 5 mg/mL). However, the ethyl acetate extract of BSNB-0294 and both xylariacein A (**8**) and B (**9**) induced an inhibition of *F. oxysporum* f. sp. *ciceris* growth (See Figure S84). On the other hand, Focicin (**12**) was tested against the endophyte Xylariaceae sp. BSNB-0294 and was not active. Focicin is a glycosylated furoic acid. Compound **12** was therefore tested on the human pathogenic strains methicillin-resistant *Staphylococcus aureus* and *Trichophyton rubrum*. This compound did not show any significant antifungal or antibacterial activity; minimal inhibitory concentrations were greater than 312 µg/mL in both cases.

It should be mentioned that neither xylariacein A (**8**) and focicin (**12**) nor extracts, fractions, or any other isolated molecules were cytotoxic to MRC-5 cells.

The isolation of xylariacein in the extract of FOCICs is directly related to the diffusion of this metabolite between the endophyte and the phytopathogen, as observed during LC-MS^2 analysis and visualization by the molecular network (Figure 1). Unlike xylariacein A, focicin

was only observed in phytopathogen extracts (alone and during the competition). Other depsipeptides were produced by the strain that were grouped in the molecular network into clusters a and b, but their production in low quantities prevented them from being isolated and formally characterized. Therefore, we hypothesized that a set of depsipeptides acting together must be responsible for the activity of endophytes. The time-dependent production of these cyclodepsipeptides by the endophyte during the interaction with the phytopathogen was studied by mass spectrometry imaging.

Mass spectrometry imaging of the dual culture between BSNB-0294 and FOCICs. A direct analysis of the competition between BSNB-0294 and FOCICs was conducted by MALDI-TOF MS imaging to monitor metabolite diffusion during coculture. MALDI-TOF images of transferred metabolites were recorded after 3, 4, 5, 6, 7, 10, and 23 days of coculture to decipher the production and diffusion of specialized metabolites (Figure S84-S86).

The study focused on the four most intense ions at *m/z* 806.46, 987.68, 1145.77, and 1286.86 (Figure 8). On day 5, the FOCICs were close enough to BSNB-0294 to suffer growth inhibition. A small diffusion of the molecule detected at *m/z* 1145.77 was concomitant with this inhibition process. At day 7, the metabolites detected at *m/z* 1145.77 (green) and 1286.88 (red) from the endophyte diffused in the culture medium and crossed the FOCIC growth border. The compound detected at *m/z* 987.68 produced by the endophyte and the compound at *m/z* 806.49 produced by the phytopathogen were only produced during the competition but were not disseminated in the medium over time (Figure S85-S88). The compound at *m/z* 987.68 was no longer produced by BSNB-0294 after 23 days (Figure S88).

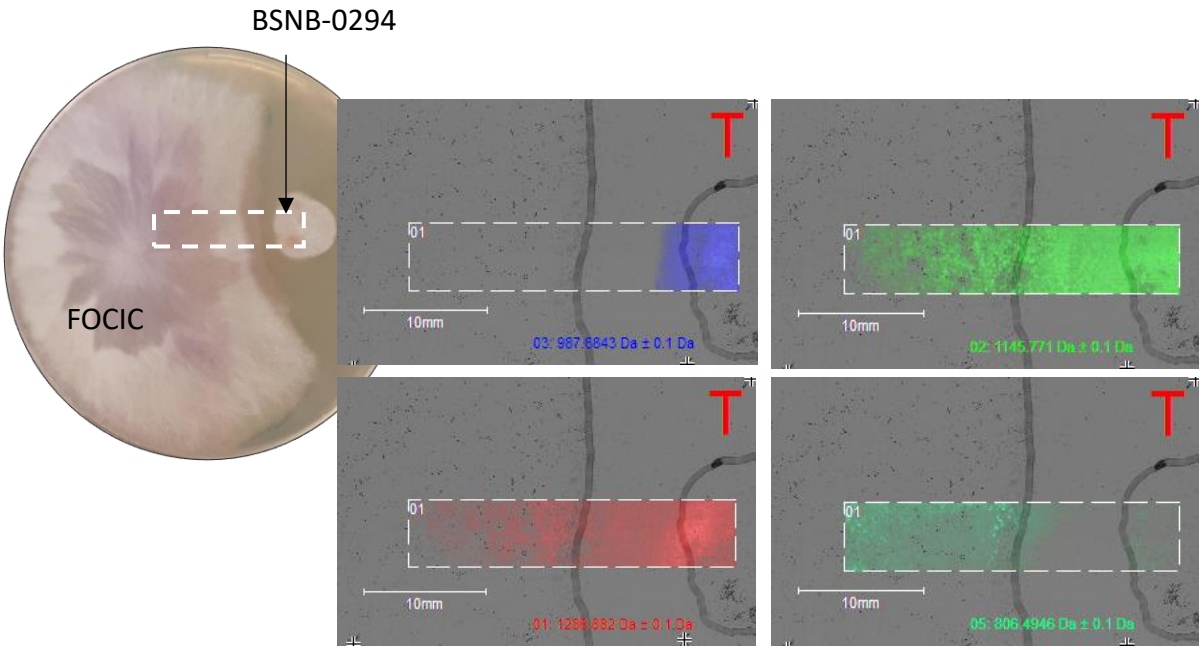

Figure 8. MALDI-TOF MS image of the competition between *F. oxysporum* f. sp. *ciceris* (left) and BSNB 0294 at seven days of coculture. The four most intense ions of the competition are mapped: *m/z* 987.68 (dark blue), 1145.77 (green), 1286.88 (red) and 806.49 (light blue). The black lines delimitate the growth areas of the two fungi.

Based on the literature related to the genus *Fusarium*, the ion at *m/z* 806.46 produced by the phytopathogen could be annotated as an analog of beauvericin in cluster c (Figure 2). The ion at *m/z* 1286.88 corresponds to sodium-cationized xylariacein A (**8**) $[M+Na]^+$ (Figures 2 and S66). The other isolated and previously identified compounds could not be detected upon imaging experiments.

These data demonstrate that FOCICs stopped growing when they encountered metabolites diffused by the endophyte BSNB-0294, especially the two metabolites detected at *m/z* 1145.77 and 1286.88.

DISCUSSION

To discover original microorganisms that naturally inhibit the phytopathogen *Fusarium oxysporum* growth, a screening of original endophytic strains library isolated from the Asteraceae *A. sciophylum* by using confrontation test was undertaken. Two fungi from the Xylariaceae family (*Muscodor* sp. BSNB-0299 and the undetermined Xylariaceae BSNB-0294) showed inhibition of the growth of two *formae speciales* of *F. oxysporum*. Among endophytes,

Xylariaceae is one of the largest and most diverse family of Ascomycota, currently comprising over 1300 accepted species, and many more remain to be discovered.[46] They are cosmopolitan, ubiquitous wood degraders, but some genera are typically encountered on dung or associated with insect nests. They clearly exhibit their highest diversity in the tropics, but new species are continuously being discovered even in temperate climate zones. Xylariaceae are among the predominant fungal endophytes of plants.[47] Thousands of orphan DNA sequences that can be assigned to this family or the order Xylariales are deposited in GenBank and other public repositories. Furthermore, Xylariaceae strains are among the most prolific producers of bioactive secondary metabolites within the fungal kingdom.[48] This taxonomic diversity of Xylariaceae strains exhibits large chemical diversity, which leads to the isolation of antibacterial or cytotoxic metabolites such as cytochalasins, xanthones, and terpenoids.[49-51] Strains from the genera *Muscodor*, *Hypoxylon*, or *Diaporthe* also produce volatile organic compounds (VOCs) against phytopathogens.[35-52] In our study, the supplementary inhibition tests carried out (face to face with *F. oxysporum*) on the first two selected Xylariaceae endophytic strains allowed to demonstrated that BSNB-0299 strain produced VOCs while the other fungi of the same genus appeared to produce non-volatile antifungals. So did the Xylariaceae BSNB-0294.

Thereafter, BSNB-0294 strain was studied by UHPLC and LC-MS/MS during confrontation with *F. oxysporum*. First of all, the stimulation of metabolite production by each strain was clearly observed but also a possible diffusion of these metabolites in the culture medium over time.

The study of specialized metabolites produced by the endophyte BSNB-0294 during confrontation with phytopathogen allowed the isolation and characterization of 9 compounds among which five (**5**-**9**) are described for the first time. The already described molecule **1** produced by the endophyte was previously isolated in a wide variety of plants and fungi,

including Xylariales species.[53] Interestingly, this compound was isolated with other analogs during competition between the endophytic fungus *Paraconiothyrium variabile* and the phytopathogen *Fusarium oxysporum*.[15] Combès *et al.* suggested that the endophyte *Paraconiothyrium variabile* also produced compound **1** when it was cocultured with *F. oxysporum* and that this compound inhibited phytopathogen growth and suppressed the production of beauvericin, a mycotoxin involved in the virulence of *F. oxysporum.*[15] Metabolite **2** was previously isolated from the fungus *Aspergillus terreus* [38] and molecule **3** from the marine sponge *Psammaplysilla purpurea*.[39] Specialized metabolites containing nitro groups as a new compounds **4** display great structural diversity, and they exhibit a wide range of biological activities, including antibiotic, antitumor, and cell signaling properties.[54] As an example, chloramphenicol (chloromycetin®) is an antibiotic produced by *Streptomyces venezuelae* and several other actinomycetes. Nitroalkyl natural products are rarer than nitroaryl compounds. 1-Nitro-2-phenylethane and 2-nitrobutylbenzene were isolated from the volatile flavor components of the African Mobola plum *Parinari curatellifolia* (Chrysobalanaceae) and identified as aroma components of tomatoes. The related compounds 1-nitro-2-(4-hydroxyphenyl)ethane and 1-nitro-2-(4-methoxyphenyl)ethane are produced as stress metabolites in leaves of the Western skunk cabbage *Lysichitum americanum* (Araceae) treated with cupric chloride. Interestingly, the last compound exhibited antifungal activities against *Fusarium oxysporum* and *Cladosporium herbarum*.[54] Based on obvious structural similarities, metabolites **2**–**4** are supposedly biosynthetic precursors of phenylalanine dimer derivatives **5**, **6**, and **7**. Compounds **4**–**7** had never been reported before in the literature. Interestingly, they are not produced in pure endophyte cultures but only when cocultures are performed. Finally, a depsipeptide named xylariacein A (**8**) was purified from Xylariaceae sp BSNB-0294 EtOAc extract and identified as the major component produced by the strain after a dual culture of three weeks. Xylariacein A is composed of 12 amino acids, seven of which are *N*-methylated.

N-Methylations are somewhat common and are performed by *N*-methyltransferase.[55] Absolute configuration was not defined despite attempted crystallization experiments. Xylariacein B was also obtained from the strain. Many cyclic depsipeptides exhibit antifungal activity against various fungi.[56-57] Xylariacein A seems to be, at least in part, responsible for the anti-phytopathogenic activity of the endophyte. In *in vitro* assays, this compound was more active than the reference antifungal used. The role of compounds **1**-**9** might be involved in virulence inhibition, as suggested by Combès *et al.* for **1**.[15] Their biological interest in endophytes has not yet been identified but must be related to the competitive environment endured by fungi.

Changes in the metabolite production of the phytopathogen also occurred during competition with BSNB-0294 endophyte. This led to identifying two known compounds already isolated from *Fusarium* genus and a new metabolite containing a glycosylated furan moiety, which was named focicin (**12**). This last compound is described here for the first time, its structure is however close to 2-furoic acid. 2-Furoic acid and some derivatives of this compound are used in the industry as preservatives, acting as bactericides and fungicides.[58] The interest for the phytopathogen strain to biosynthesize focicin as well as the role of this compound during an interaction remains to be determined.

Although many compounds have already been described and isolated from *Fusarium* sp. and Xylariaceae strains,[53,59] it was possible to identify new compounds in these two species by using OSMAC method, *i.e.* confrontation between phytopathogenic and endophytic strain in our case. It seems that these compounds are more produced during the confrontation and act as antagonist molecules.

MALDI-TOF MS imaging analyses were performed to understand when and how these compounds are produced during interspecies chemical interaction. Xylariacein A was produced by BSNB-0294 in high level and diffused in the culture media after 6 days of coculture with *F.*

oxysporum and inhibited the growth of *F. oxysporum* confirming that it is an antagonistic compound. For the other identified compounds, this point remains to be determined.

CONCLUSION

Fusoriosis, a plant disease related to fungi of *Fusarium* genera, causes major production losses in agriculture. It is essential to be able to fight against such diseases either by biocontrol agents or by new phytosanitary products. Our results are encouraging in both of these fields and will serve as a basis for further field studies.

The exploration of the chemical space of BSNB-0294 strain (Xylariaceae) secondary metabolites, by the combination of metabolomics and OSMAC strategy led to isolate 12 compounds. During the interspecific competition, 6 molecules were isolated and identified from the endophyte and 3 characterized from the phytopathogen. Among all of these compounds, 6 are described for the first time. The ecological role of all identified metabolites remains unknown and will be undertaken. However, it was possible to determine that Xylariacein A induce an inhibition growth of *F. oxypsorum*. It was also possible to follow the biosynthesis during confrontation of this polypeptide produced by the endophyte and diffuse in the medium over time. To date, it is reasonable to consider the xylariacein-type peptides or the use of BSNB-0294 directly on crops to fight fusariosis.

ASSOCIATED CONTENT

Supporting Information.

This information is available free of charge via the Internet at http://pubs.acs.org.

AUTHOR INFORMATION

Corresponding Author

*Tel: +33 169 823 679. E-mail: veronique.eparvier@cnrs.fr and +33 169 823 032. E-mail: david.touboul@cnrs.fr.

Author Contributions

The manuscript was written through contributions of all authors. All authors have given approval to the final version of the manuscript. These authors contributed equally.

Notes

The authors declare no competing financial interest.

ACKNOWLEDGMENTS

We would like to thank Dr. Katia Gindro from the Geneva Agroscope for providing us the *Fusarium oxysporum* f.sp. *ciceris* phytopathogen.

FUNDING SOURCES

This work was supported by Agence Nationale de la Recherche - Swiss National Science Foundation (ANR-SNF) grant (SECIL, ref ANR-15-CE21-0016 and SNF N° 310030E-164289) and from an "Investissement d'Avenir" grant (CEBA, ref ANR-10-LABX-0025) managed by the ANR.

REFERENCES

1. Ortoneda, M; Guarro, J.; Madrid, M.P.; Caracuel, Z.; Roncero, M.ILG.; Mayayo, E.; Di Pietro, A. *Fusarium oxysporum* as a multihost model for the genetic dissection of fungal virulence in plants and mamals. *Infect. Immun.* **2004,** *72*, 1760–1766.

2. Michielse, C.B.; Rep, M. Pathogen profile update: *Fusarium oxysporum*. *Mol. Plant Pathol.* **2009,** *10*, 311–3424.

3. Fravel, D.; Olivain, C.; Alabouvette, C. *Fusarium oxysporum* and its biocontrol. *New Phytologist* **2003,** *157* (3), 493–502.

4. Kistler, H. C. Evolution of host specificity in *Fusarium oxysporum*. In *Fusarium: Paul E. Nelson Memorial Symposium.*, Society, T. A. P., Ed. B.A. Summerell, J.F. Leslie, D. Backhouse, W.L. Bryden and L.W. Burgess: St. Paul, 2001; pp 70–82.

5. Ploetz, R. C. Panama disease: a classic and destructive disease of banana. *Plant Health Prog.* **2000,** *1*, 10.

6. Fourie, G.; Steenkamp, E. T.; Ploetz, R. C.; Gordon, T. R.; Viljoen, A. Current status of the taxonomic position of *Fusarium oxysporum* formae specialis *cubense* within the *Fusarium oxysporum* complex. *Infect. Genet. Evol.* **2011,** *11*, 533–542.

7. Edel-Hermann, V.; Lecomte, C. Current status of *Fusarium oxysporum* formae speciales and races. *Phytopathology* **2018,** *109*, 512–530.

8. Nel, B.; Steinberg, C.; Labuschagne, N.; Viljoen, A. Evaluation of fungicides and sterilants for potential application in the management of *Fusarium* wilt of banana. *Crop Prot.* **2007,** *26*, 697–705.

9. Bennett, R. S.; Spurgeon, D. W.; DeTar, W. R.; Gerik, J. S.; Hutmacher, R. B.; Hanson, B. D. Efficacy of four soil treatments against *Fusarium oxysporum* f. sp. *vasinfectum* race 4 on cotton. *Plant Dis.* **2011,** *95*, 967–976.

10. Amini, J.; Sidovich, D. The effects of fungicides on *Fusarium oxysporum* f. sp. *lycopersici* associated with *Fusarium* wilt of tomato. *J. Plant Prot. Res.* **2010,** *50*, 172–178.

11. Ploetz, R. *Fusarium* Wilt of Banana is Caused by Several Pathogens Referred to as *Fusarium oxysporum* f. sp. *cubense*. *Phytopathology* **2006,** *96* (6), 653–656.

12. Yadeta, F.A.; Thomma, B.P.H.J. The xylem as battleground for plant hosts ans vascular wilt pathogens. *Front. Plant Sci.* **2013,** *4*, 786–791.

13. Jie, L.; Zifeng, W.; Lixiang, C.; Hongming, T.; Patrik, I.; Zide, J.; Shining, Z. Artificial inoculation of banana tissue culture plantlets with indigenous endophytes originally derived from native banana plants. *Biol. Control* **2009,** *51*, 427–434.

14. Oshiro, K. G. N.; Rodrigues, G.; Monges, B. E. D.; Cardoso, M. H.; Franco, O. L. Bioactive peptides against fungal biofilms. *Front. Microbiol.* **2019,** *10*, 2169.

15. Combès, A.; Ndoye, I.; Bance, C.; Bruzaud, J.; Djediat, C.; Dupont, J.; Nay, B.; Prado, P., Chemical communication between the endophytic fungus *Paraconiothyrium variabile* and the phytopathogen *Fusarium oxysporum*. *PLoS One* **2012,** *7* (10), e47313.

16. Fierro-Cruz, J. E.; Jiménez, P.; Coy-Barrera, E. Fungal endophytes isolated from *Protium heptaphyllum* and Trattinnickia rhoifolia as antagonists of *Fusarium oxysporum*. *Revista Argentina de Microbiología* **2017,** *49* (3), 255-263.

17. Terhonen, E.; Sipari, N.; Asiegbu, F. O. Inhibition of phytopathogens by fungal root endophytes of Norway spruce. *Biol. Control* **2016,** *99*, 53-63.

18. Netzker, T.; Fischer, J.; Weber, J.; Mattern, D. J.; König, C. C.; Valiante, V.; Schroeckh, V.; Brakhage, A. A. Microbial communication leading to the activation of silent fungal secondary metabolite gene clusters. *Front Microbiol.* **2015,** *20* (6), 299.

19. Hewage, R. T.; Aree, T.; Mahidol, C.; Ruchirawat, S.; Kittakoop, P. One strain-many compounds (OSMAC) method for production of polyketides, azaphilones, and an isochromanone using the endophytic fungus Dothideomycete sp. *Phytochemistry* **2014,** *108*, 87-94.

20. Bode, H. B.; Bethe, B.; Höfs, R.; Zeeck, A. Big effects from small changes: possible ways to explore nature's chemical diversity. *Chem. Bio. Chem.* **2002,** *3*, 619–627.

21. Wakefield, J.; Hassan, H. M.; Jaspars, M.; Ebel, R.; Rateb, M. E. Dual induction of new microbial secondary metabolites by fungal bacterial co-cultivation. *Front. Microbiol.* **2017,** *11* (8), 1284.

22. Bertrand, S.; Schumpp, O.; Bohni, N.; Monod, M.; Gindro, K.; J-L., W. De novo production of metabolites by fungal co-culture of *Trichophyton rubrum* and *Bionectria ochroleuca*. *J. Nat. Prod.* **2013,** *76*, 1157-1165.

23. Barthélemy, M.; Elie, N.; Pellissier, L.; Wolfender, J.-L.; Stien, D.; Touboul, D.; Eparvier, V. Structural identification of antibacterial lipids from Amazonian palm tree endophytes through the Molecular Network approach. *Int. J. Mol. Sci.* **2019,** *20*, 1083.

24. Charles-dominique, P.; Chave, J.; Dubois, M. A.; De Granville, J.-J.; Riera, B.; Vezzoli, C. Colonization front of the understorey palm *Astrocaryum sciophilum* in a pristine rain forest of French Guiana. *Global Ecol. Biogeogr.* **2003,** *12*, 237–248.

25. Alvarez-Sanchez, J.; Barajas-Guzman, G.; Campo, J.; Leon, R., Inorganic nitrogen and phosphorus in stemflow of the palm *Astrocaryum mexicanum* Liebm. located in Los Tuxtlas, Mexico. *Trop. Ecol.* **2106,** *57*, 45-55.

26. Vallet, M.; Vanbellingen, Q. P.; Fu, T.; Le Caer, J. P.; Della-Negra, S.; Touboul, D.; Duncan, K. R.; Nay, B.; Brunelle, A.; Prado, S. An integrative approach to decipher the chemical antagonism between the competing endophytes *Paraconiothyrium variabile* and *Bacillus subtilis*. *J. Nat. Prod.* **2017,** *80* (11), 2863-2973.

27. Song, C.; Mazzola, M.; Cheng, X.; Oetjen, J.; Alexandrov, T.; Dorrestein, P.; Watrous, J.; van der Voort, M.; Raaijmakers, J. M. Molecular and chemical dialogues in bacteria-protozoa interactions. *Sci Rep* **2015,** *6* (5), 12837.

28. Casella, T.M.; Eparvier, V.; Mandavid, H.; Bendelac, A.; Odonne, G.; Dayan, L.; Duplais, C.; Espindola, L.S.; Stien ,D. Antimicrobial and cytotoxic secondary metabolites from tropical leaf endophytes: Isolation of antibacterial agent pyrrocidine C from *Lewia infectoria* SNB-GTC2402. *Phytochemistry* **2013,** *96*, 370-377.

29. Clinical and Laboratory Standards. Methods for Dilution Antimicrobial Susceptibility Tests for Bacteria That Grow Aerobically - M07. Wayne, PA, USA 2018; Vol. 11th.

30. Tempête, C.; Werner, G.; Favre, F.; Rojas, A.; Langlois, N. In vitro cytostatic activity of 9-demethoxyporothramycin B. *Eur. J. Med. Chem.* **1995,** *30* (7), 647-650.

31. Olivon, F.; Allard, P. M.; Koval, A.; Righi, D.; Genta-Jouve, G.; Neyts, J.; Apel, C.; Pannecouque, C.; Nothias, L. F.; Cachet, X.; Marcourt, L.; Roussi, F.; Katanaev, V. L.; Touboul, D.; Wolfender, J. L.; Litaudon, M. Bioactive natural products prioritization using massive multi-informational molecular networks. *ACS Chem Biol.* **2017,** *12*, 2644-2651.

32. Myers, O. D.; Sumner, S. J.; Li, S.; Barnes, S.; Du, X. One step forward for reducing false positive and false negative compound identifications from mass spectrometry metabolomics data: new algorithms for constructing extracted ion chromatograms and detecting chromatographic peaks. *Anal. Chem.* **2017,** *89* (17), 8696-8703.

33. Olivon, F.; Elie, N.; Grelier, G.; Roussi, F.; Litaudon, M.; Touboul, D. MetGem software for the generation of molecular networks based on the t-SNE algorithm. *Anal Chem* **2018,** *90*, 13900-13908.

34. Donald, J.; Barthélemy, M.; Gazal, N.; Eveno, Y.; Manzi, S.; Eparvier, V.; Stien, D.; Roy, M. Tropical palm endophytes exhibit low competitive structuring when assessed using co-occurrence and antipathogen activity analysis. *Front. For. Global Change* **2019,** *2*, 86.

35. Pena, L. C.; Jungklaus, G. H.; Savi , D. C.; Ferreira-Maba, L.; Servienski, A.; Maia, B. H. L. N. S.; Annies, V.; Galli-Terasawa, L. V.; Glienke, C.; Kava, V., *Muscodor brasiliensis* sp. nov. produces volatile organic compounds with activity against *Penicillium digitatum*. *Microbiol. Res.* **2019,** *221*, 28–35.

36. Olivon, F.; Grelier, G.; Roussi, F.; Litaudon, M.; Touboul, D. MZmine 2 data-preprocessing to enhance molecular networking reliability. *Anal. Chem.* **2017,** *89*, 7836–7840.

37. Prado, S.; Buisson, D.; Ndoye, N.; Vallet, M.; Nay, B. One-step enantioselective synthesis of (4S)-isosclerone through biotranformation of juglone by an endophytic fungus. *Tet. Lett.* **2013,** *54* (10), 1189-1191.

38. Guo, C.-J.; Yeh, H.-H.; Chiang, Y.-M.; Sanchez, J. F.; Chang, S.-L.; Bruno, K. S.; Wang, C. C. C., Biosynthetic pathway for the Epipolythiodioxopiperazine acetylaranotin in

Aspergillus terreus revealed by genome-based deletion analysis. *J. Am. Chem. Soc.* **2013,** *135*, 7205–7213.

39. Yagi, H.; Matsunaga, S.; Fusetani, N., Purpuramines A-I New bromotyrosiae-derived metabolites from the marine sponge *Fsammuplysilla purpurea*. *Tehtrahedron* **1993,** *49*, 3749-3754.

40. Huang, L-H.; Chen, Y-X.; Yu, J-C.; Li, H-J.; Ma, W-Z.; Watanapokasin, R.; Hu, K-C.; Niaz, S.I.; Yang, D-P.; Lan, W-J. Secondary metabolites from the marine-derived fungus *Dichotomyces* sp. L-8 and their cytotoxic activity. *molecules* **2017,** *22*, 444.

41. Langhanki, J.; Rudolph, K.; Erkel, G.; Opatz, T. Total synthesis and biological evaluation of the natural product (−)-cyclonerodiol, a new inhibitor of IL-4 signaling. *Org. Biomol. Chem.* **2014,** *12*, 9707–9715.

42. Deng, Z.; Li, C.; Luo, D.; Teng, P.; Guo, Z.; Tu, X.; Zouy, K.; Gong, D. A new cinnamic acid derivative from plant-derived endophytic fungus *Pyronema* sp.. *Nat. Prod. Res.* **1995,** *31* (20), 2413-2419.

43. Laurent, D.; Goasdoue, N.; Kohler, F.; Pellegrin, F.; Platzer, N. Characterization of cyclonerodiol isolated from corn infested by *Fusarium moniliforme* Sheld.: One- and two-dimensional 1H and 13C NMR study. *Magn. Reson. Chem.* **1990,** *28*, 662-664.

44. Smith, S. G.; Goodman, J. M. Assigning stereochemistry to single diastereoisomers by GIAO NMR Calculation: The DP4 Probability. *J. Am. Chem. Soc.* **2010,** *132* (37), 12946−12959.

45. Davey, S. Through the looking glass. *Nat. Chem.* **2014,** *6* (2), 87-87.

46. Stadlera, M.; Kuhnerta, E.; Peršohb, D.; Fournierc, J. The Xylariaceae as model example for a unified nomenclature following the “One Fungus-One Name” (1F1N) concept *Mycology* **2013,** *4*(1), 5-21.

47. Rogers, J. D. Thoughts and musings on tropical Xylariaceae. *Mycol. Res.* **2000,** *104*, 1412–1420.

48. Stadler, M.; Hellwig, V. Chemotaxonomy of the Xylariaceae and remarkable bioactive compounds from Xylariales and their associated asexual states. *Recent Res. Devel. Phytochem.* **2005,** *9*, 41–93.

49. Rudiyansyah; Alimuddin, A. H.; Masriani; Muharini, R.; Liu, Z.; Lin, W.; Hartmann, R.; Proksch, P. Arugosins O-Q, new fungal metabolites from the fungus Xylariaceae sp. isolated from leaves of *Lansium domesticum* (Meliaceae). *Nat. Prod. Commun.* **2019,** *14* (1), 125-128.

50. Mühlbauer, A.; Triebel, D.; Persoh, D.; Wollweber, H.; Seip, S.; Stadler, M. Macrocarpones, novel metabolites from stromata of *Hypoxylon macrocarpum*, and new evidence on the chemotaxonomy of *Hypoxylon* species. *Mycol. Prog.* **2002,** *1*, 235–248.

51. Malet-Cascón, L.; Romero, F.; Espliego-Vázquez, F.; Grávalos, D.; Fernández-Puentes, J. L. IB-00208, a new cytotoxic polycyclic xanthone produced by a marine-derived *Actinomadura*. *J. Antibiot.* **2003,** *56*, 219–225.

52. Daisy, B. H.; Strobel, G. A.; Castillo, U.; Ezra, D.; Sears, J.; Weaver, D. K.; Runyon, J. B. Naphthalene, an insect repellent, is produced by *Muscodor vitigenus*, a novel endophytic fungus. *Microbiology* **2002,** *148*, 3737–3741.

53. Becker, K.; Stadler, M. Recent progress in biodiversity research on the Xylariales and theur secondaru metabolism. *J. Antibiot.* **2021,** *74*, 1–23.

54. Parry, R.; Nishino, S.; Spain, J. Naturally-occurring nitro compounds. *Nat. Prod. Rep.* **2011,** *28*, 152-167.

55. Dewick, P. M. *Medicinal Natural Products - A biosynthetic approach*. Third ed.; 2008.

56. Sivanathan, S.; Scherkenbeck, J. Cyclodepsipeptides: A rich source of biologically active compounds for drug research. *Molecules* **2014,** *19*, 12368–12420.

57. Olleik, H.; Nicoletti, C.; Lafond, M.; Courvoisier-Dezord, E.; Xue, P.; Hijazi, A.; Baydoun, E.; Perrier, J.; Maresca, M. Comparative Structure–Activity Analysis of the Antimicrobial Activity, Cytotoxicity, and Mechanism of Action of the Fungal Cyclohexadepsipeptides Enniatins and Beauvericin. *Toxins* **2019,** *11*, 514.

58. National Library of Medicine, National Center for Biotechnology Information. https://pubchem.ncbi.nlm.nih.gov/compound/2-Furoic-acid. (accessed 22 january 2021).

59. Li, M.; Yu, R.; Bai, X.; Wang, H.; Zhang, H. *Fusarium*: atreasure trove of bioactive secondary metabolites. *Nat. Prod. Rep.* **2020,** *37*, 1568–1588.

FOR TABLE OF CONTENTS ONLY